Zhu, D. *et al*. (2017). *Géotechnique* **67**, No. 8, 733–746 [http://dx.doi.org/10.1680/jgeot.16.P.223]

TECHNICAL NOTE

Probabilistic stability analyses of undrained slopes with linearly increasing mean strength

D. ZHU*, D. V. GRIFFITHS†, J. HUANG‡ and G. A. FENTON§

Based on recently published deterministic solutions as a benchmark, the random finite-element method is used here to investigate the influence of spatial variability on the undrained stability of normally consolidated random slopes, where the mean strength increases linearly with depth while the coefficient of variation remains constant. Results are presented in the form of charts that give the mean and standard deviation of a dimensionless stability number. Using the charts presented in this note, engineers can obtain a preliminarily assessment of the probability of failure of normally consolidated clay slopes.

KEYWORDS: clays; failure; finite-element modelling; shear strength; slopes; statistical analysis

INTRODUCTION

In the realm of probabilistic geotechnical analysis, slope stability analysis seems to have received more attention in the literature than any other geotechnical application. Important early probabilistic works appeared in the 1970s (e.g. Matsuo & Kuroda, 1974; Alonso, 1976; Tang *et al*., 1976; Vanmarcke, 1977) and papers have continued steadily. Recognition that geotechnical engineering is highly amenable to probabilistic treatment goes back much further. In his foreword to the inaugural issue of *Géotechnique*, Terzaghi (1948) wrote about the properties of the soil material varying 'from point to point'. Various probabilistic methods have been developed for predicting the reliability of geotechnical structures, such as event trees, first-order second-moment (FOSM) method and first-order reliability method (FORM) (e.g. Whitman, 1984; Christian *et al*., 1994; Lacasse, 1994; Wolff, 1996; Hassan & Wolff, 1999; Duncan 2000).

It is only relatively recently, however, that Terzaghi's (1948) observation of spatial variability of soil properties has been tackled explicitly by an advanced numerical method called the random finite-element method (RFEM), with initial application to seepage problems (Fenton & Griffiths, 1993; Griffiths & Fenton, 1993), and later to slope stability analysis (e.g. Griffiths & Fenton, 2000, 2004; Griffiths *et al*., 2009). In these studies, slope stability was investigated systematically using elastic–plastic finite-element methodologies combined with random field theory in a Monte-Carlo framework. The random fields were generated by the local averaging subdivision (LAS) method (Fenton & Vanmarcke, 1990), which fully accounts for spatial variability and local averaging over each finite element. All the RFEM analyses mentioned previously considered slopes with stationary random properties; that is, the mean and standard deviation of strength were spatially constant. Owing to the influence of the effective overburden pressure, however, normally consolidated clays regularly display an increasing undrained strength trend with depth. This problem has received considerable attention in the past deterministically (e.g. Gibson & Morgenstern, 1962; Hunter & Schuster, 1968; Koppula, 1984; Yu *et al*., 1998; USACE, 2003; Griffiths & Yu, 2015). In the framework of probabilistic analysis, Hicks & Samy (2002) considered some non-stationary random slopes using RFEM for the special case of zero strength at the ground surface (e.g. Gibson & Morgenstern, 1962), while Griffiths *et al*. (2015) introduced briefly the broader class of slopes in which the mean strength increases linearly with depth from a non-zero value at the ground surface (e.g. Hunter & Schuster, 1968). This note will extend the work of Griffiths *et al*. (2015) and present a comprehensive set of results, together with a detailed description of the algorithm for achieving the non-stationary random field.

The problem definition is shown in Fig. 1, where the slope angle is β, the slope height is H and the depth ratio to a firm stratum is D. The mean undrained strength is a linear function of depth given by the equation

$$\mu_{c_{uz}} = \mu_{c_{u0}} + \rho z \tag{1}$$

where $\mu_{c_{uz}}$ is the mean strength at depth z and $\mu_{c_{u0}}$ is the mean strength at the crest level. ρ is the gradient of mean strength increase with z, with typical values varying from slightly greater than 0 to 3·5 kN/m^3 (e.g. Koppula, 1984). In this study the standard deviation of strength is also assumed to be proportional to depth with a gradient that results in a constant coefficient of variation v_{c_u} (e.g. Lumb, 1966). For random field modelling, the spatial correlation length is given by θ, and for the purpose of parametric studies, a dimensionless spatial correlation length Θ is used where $\Theta = \theta/H$. Deterministic parameters include the undrained friction angle, $\phi_u = 0$, and the saturated unit weight, γ.

Manuscript received 23 August 2016; revised manuscript accepted 12 January 2017. Published online ahead of print 15 February 2017. Discussion on this paper closes on 1 January 2018, for further details see p. ii.

* Key Laboratory of Ministry of Education for Geomechanics and Embankment Engineering, Hohai University, Nanjing, P. R. China.
† Department of Civil and Environmental Engineering, Colorado School of Mines, Golden, CO, USA.
‡ Australian Research Council Centre of Excellence for Geotechnical Science and Engineering, University of Newcastle, Callaghan, NSW, Australia.
§ Department of Engineering Mathematics, Dalhousie University, Halifax, NS, Canada.

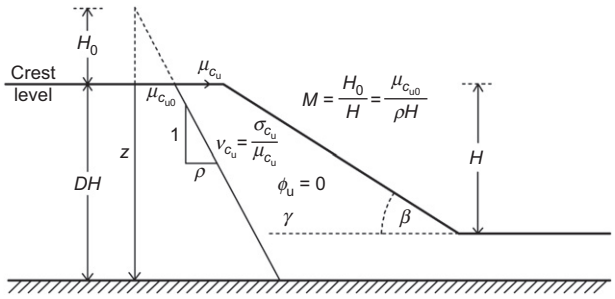

Fig. 1. Random slope with linearly increasing mean strength

NON-STATIONARY RANDOM FIELD GENERATION

Some investigators have looked into non-stationary random field of soil properties; for example, Li *et al.* (2014) investigated the reliability of infinite slopes with linearly increasing mean strength; Li *et al.* (2015) investigated the reliability of a strip footing in the presence of spatially variable undrained shear strength that linearly increases with depth; and Müller *et al.* (2016) focused on the reliable assessment of a staged embankment construction. Non-stationary random fields are used throughout the present study of two-dimensional (2D) slope stability, using the following algorithm based on initial generation and subsequent adjustment of a stationary random field.

With reference to Fig. 1, a random field with the properties given by equation (1) can be generated using the following steps.

Step 1: initially generate a homogeneous stationary lognormal random field across the mesh based on the parameters at $z = 0$, namely, the mean, $\mu_{c_{u0}}$, standard deviation, $\sigma_{c_{u0}}$ and spatial correlation length, θ. Let the initial values assigned to all elements at this stage be c_{0i}, $i = 1, 2, \ldots, n$ where n is the number of elements in the mesh.

Step 2: the element values are then adjusted to account for depths $z > 0$ using the scaling factor

$$c_{zi} = c_{0i}\frac{\mu_{c_{u0}} + \rho z}{\mu_{c_{u0}}}, \quad i = 1, 2, \ldots, n \tag{2}$$

where z is sampled at the centroid of each element. For details of the derivation of equation (2), see the Appendix.

Figure 2 shows a typical realisation of a random field with the properties indicated in the figure caption. Dark and light regions depict high and low values of soil strength, respectively. It can be seen from Fig. 2 that the grey-scale is becoming darker as the soil strengthens with increased depth, z.

It should be noted that, if $\rho = 0$, no adjustment in step 2 is necessary, and the stationary random field generated in step 1 is retained. The case of stationary random fields in slope stability analysis was reported in detail by Griffiths & Fenton (2004), who also presented an analytical solution corresponding to the case of an infinite spatial correlation length. The analytical solution was shown to lead to unconservative results in some cases (i.e. underestimates of probability of failure p_f values). The reader is also referred to this paper for further discussion on the influence of spatial correlation length on probabilistic outcomes in slope stability analysis.

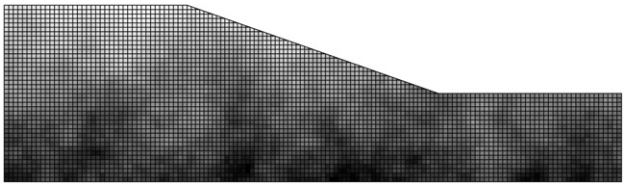

Fig. 2. A typical realisation of a random field for a slope with $\beta = 20°$, $M = 1{\cdot}0$, $D = 2{\cdot}0$, $v_{c_u} = 0{\cdot}1$ and $\Theta = 1{\cdot}0$

RESULTS OF RFEM ANALYSES

Recent solutions of the deterministic slope stability problem shown in Fig. 1 (Griffiths & Yu, 2015) have refined the charts of Hunter & Schuster (1968). The fundamental solution is a stability number N expressed as

$$N = f(\beta, D, M) \tag{3}$$

where M is a dimensionless strength gradient parameter defined as

$$M = \frac{\mu_{c_{u0}}}{\rho H} = \frac{H_0}{H} \tag{4}$$

The factor of safety, FS, is proportional to the stability number, N, given by

$$\mathrm{FS} = N\frac{\rho}{\gamma} \tag{5}$$

or

$$N = \mathrm{FS}\frac{\gamma}{\rho} \tag{6}$$

In the context of a Monte-Carlo analysis, each realisation of an RFEM analysis of the problem shown in Fig. 1 involves generation of a non-stationary random field as described in the previous section, followed by a conventional deterministic slope stability analysis using strength reduction to compute the factor of safety, FS. Finally the stability number N is retrieved from equation (6). The process is then repeated; a new non-stationary random field is generated, leading to a different stability number N and so on. Following a suite of Monte-Carlo simulations, the mean and standard deviation of the stability number (μ_N and σ_N) for different parametric combinations can be determined, and have been plotted in Figs 3–6. In the current study, 1000 Monte-Carlo simulations were considered enough to give reasonably stable and reproducible statistical output. Fig. 7 shows μ_N and σ_N as a function of the number of simulations for a typical slope example, indicating that stable results occur as the number of simulations reaches $n_{sim} = 1000$.

In each of the charts presented in Figs 3–6, the abscissa is the depth ratio D, the ordinate to the left is μ_N and the ordinate to the right is σ_N. Consider, for example, a slope with $M = 0{\cdot}5$, $\beta = 15°$ and $\Theta = 0{\cdot}5$, as shown in Fig. 8. As might be expected, for slopes with low values of the coefficient of variation, the mean stability numbers agree well with the results from deterministic analysis. For higher values of the coefficient of variation, the mean stability numbers decrease, implying a decreasing value of the mean factor of safety. An interesting observation from Fig. 8 is that the mean stability number for higher values of v_{c_u} continues to fall with increasing depth ratio (in the range $1{\cdot}5 < D < 2{\cdot}0$) where the deterministic results would remain constant. This phenomenon emphasises the 'seeking out' effect of the critical failure mechanism in a finite-element slope stability analysis. Fig. 9 shows three failure mechanisms from a suite of Monte-Carlo simulations for the same case with $v_{c_u} = 0{\cdot}5$ and $D = 2{\cdot}0$. In the deterministic case with $M = 0{\cdot}5$ and $\beta = 15°$, the mechanism can never go deeper than $D = 1{\cdot}5$ (see Fig. 5(b) in Griffiths & Yu (2015)); however, in some of the probabilistic simulations, the failure mechanism does go

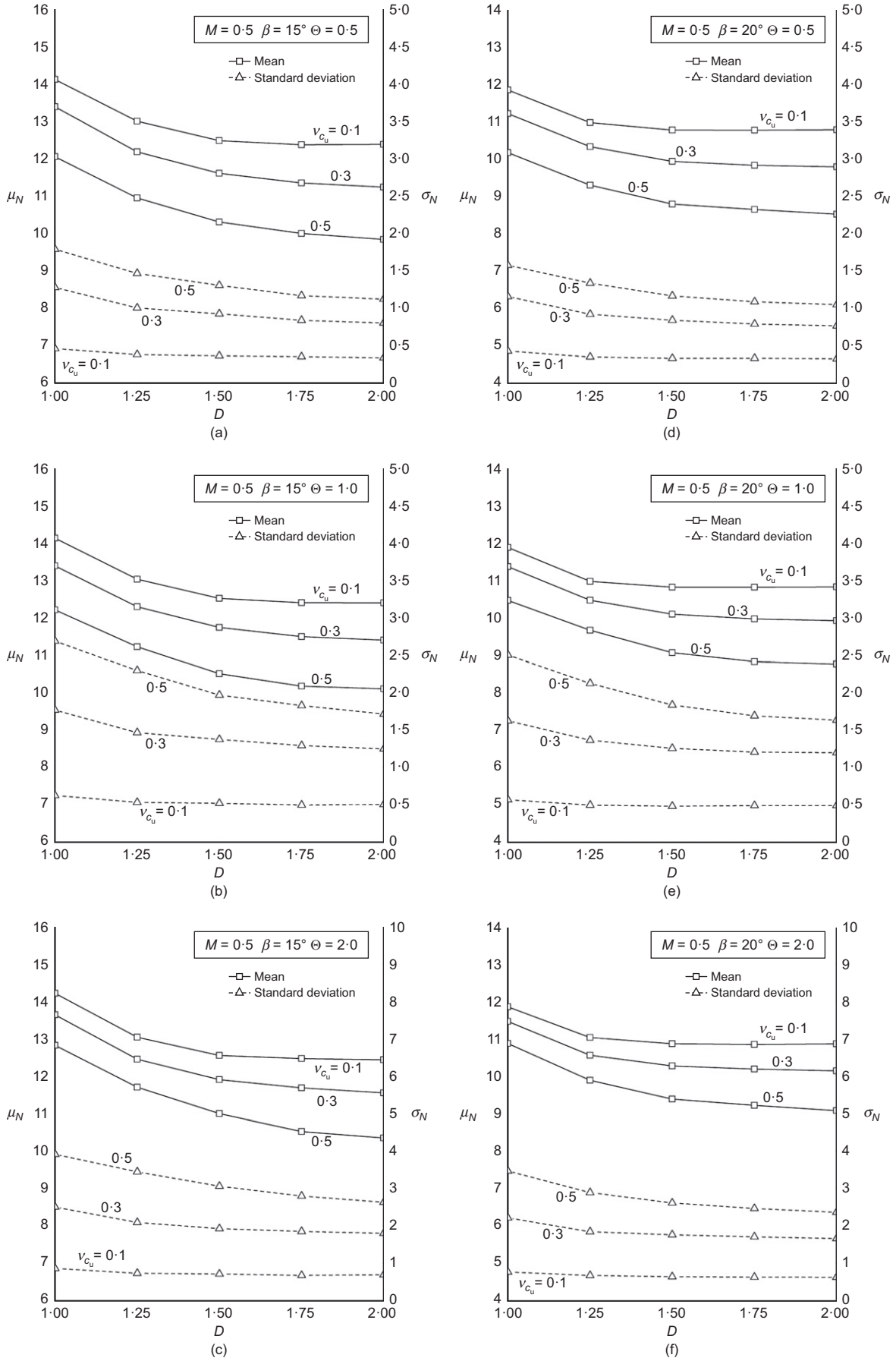

Fig. 3. Mean and standard deviation of stability number (μ_N and σ_N) against depth ratio (D) for $M = 0{\cdot}5$: (a) $\beta = 15°$ and $\Theta = 0{\cdot}5$; (b) $\beta = 15°$ and $\Theta = 1{\cdot}0$; (c) $\beta = 15°$ and $\Theta = 2{\cdot}0$; (d) $\beta = 20°$ and $\Theta = 0{\cdot}5$; (e) $\beta = 20°$ and $\Theta = 1{\cdot}0$; (f) $\beta = 20°$ and $\Theta = 2{\cdot}0$; (g) $\beta = 30°$ and $\Theta = 0{\cdot}5$; (h) $\beta = 30°$ and $\Theta = 1{\cdot}0$; (i) $\beta = 30°$ and $\Theta = 2{\cdot}0$; (j) $\beta = 40°$ and $\Theta = 0{\cdot}5$; (k) $\beta = 40°$ and $\Theta = 1{\cdot}0$; (l) $\beta = 40°$ and $\Theta = 2{\cdot}0$ (continued on next page)

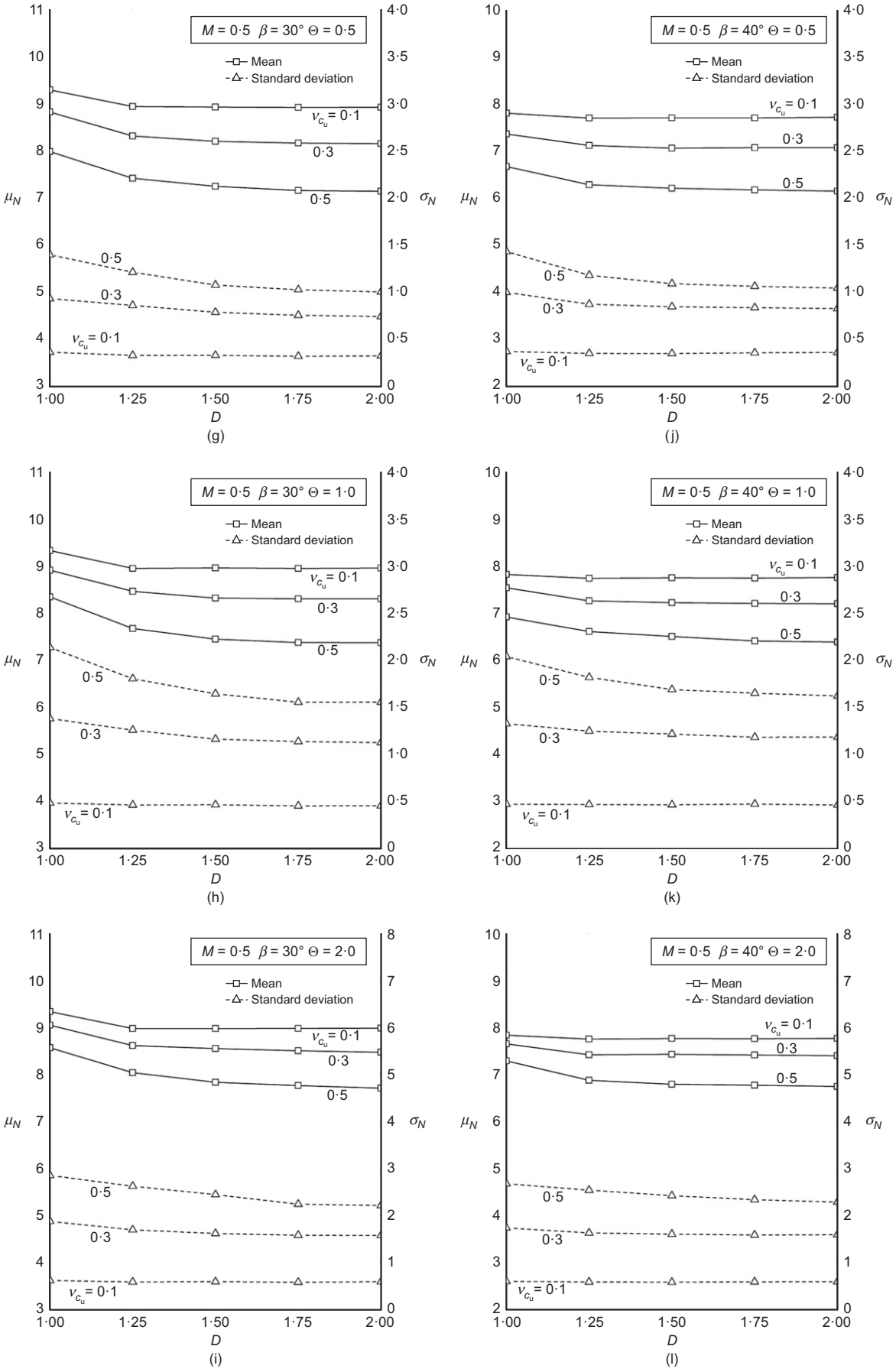

Fig. 3. Continued

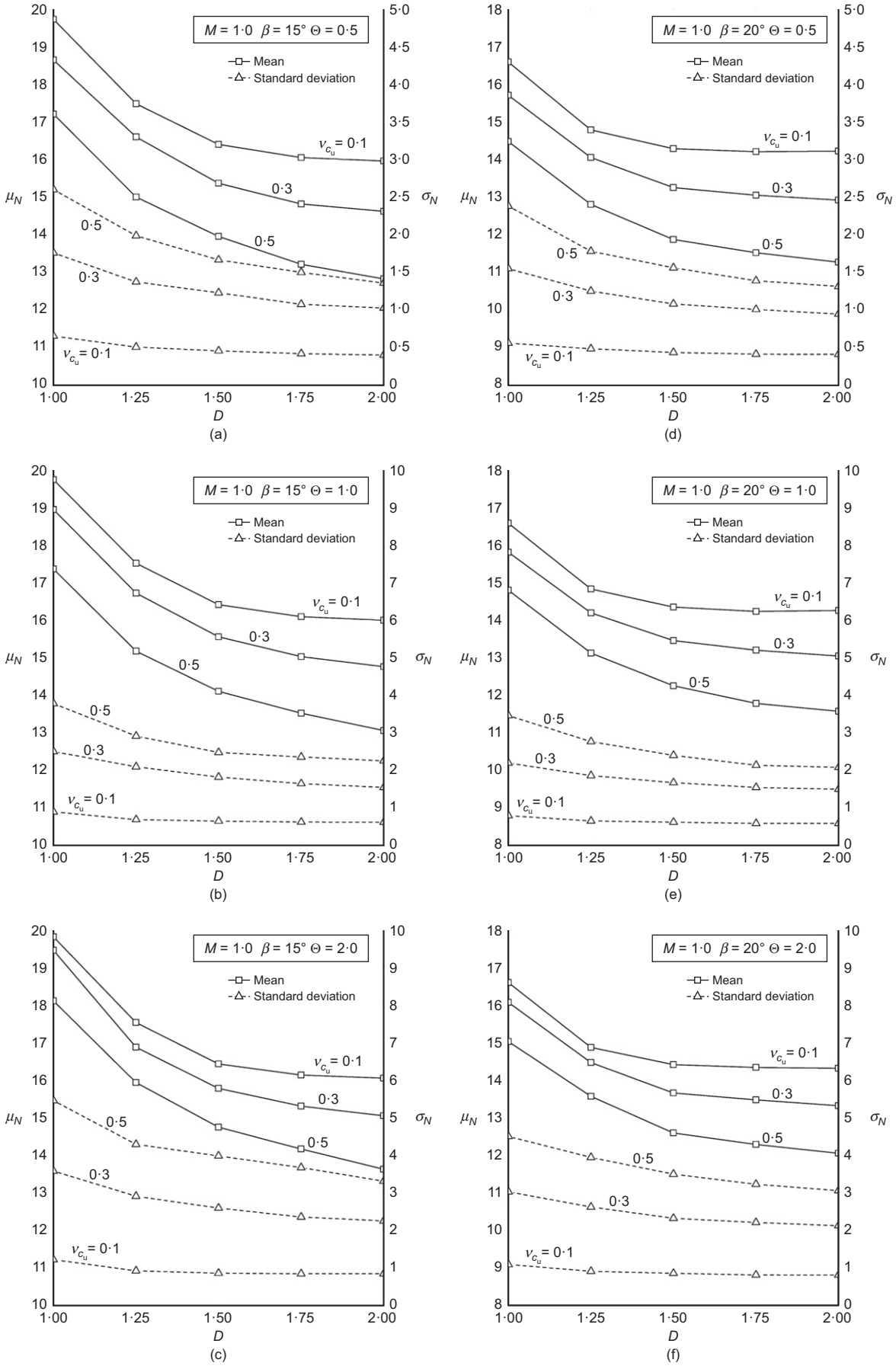

Fig. 4. Mean and standard deviation of stability number (μ_N and σ_N) against depth ratio (D) for $M = 1{\cdot}0$: (a) $\beta = 15°$ and $\Theta = 0{\cdot}5$; (b) $\beta = 15°$ and $\Theta = 1{\cdot}0$; (c) $\beta = 15°$ and $\Theta = 2{\cdot}0$; (d) $\beta = 20°$ and $\Theta = 0{\cdot}5$; (e) $\beta = 20°$ and $\Theta = 1{\cdot}0$; (f) $\beta = 20°$ and $\Theta = 2{\cdot}0$; (g) $\beta = 30°$ and $\Theta = 0{\cdot}5$; (h) $\beta = 30°$ and $\Theta = 1{\cdot}0$; (i) $\beta = 30°$ and $\Theta = 2{\cdot}0$; (j) $\beta = 40°$ and $\Theta = 0{\cdot}5$; (k) $\beta = 40°$ and $\Theta = 1{\cdot}0$; (l) $\beta = 40°$ and $\Theta = 2{\cdot}0$ (continued on next page)

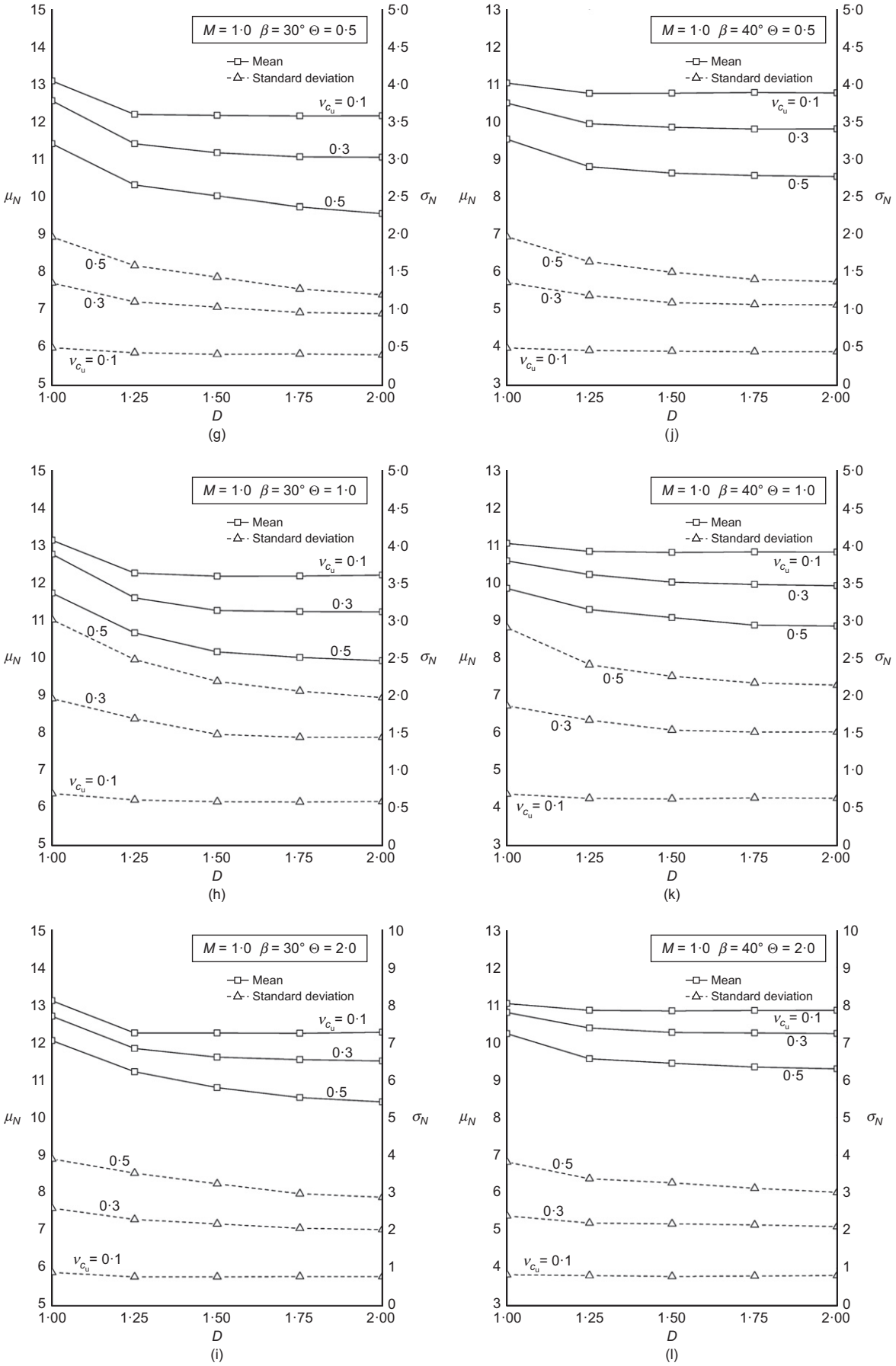

Fig. 4. Continued

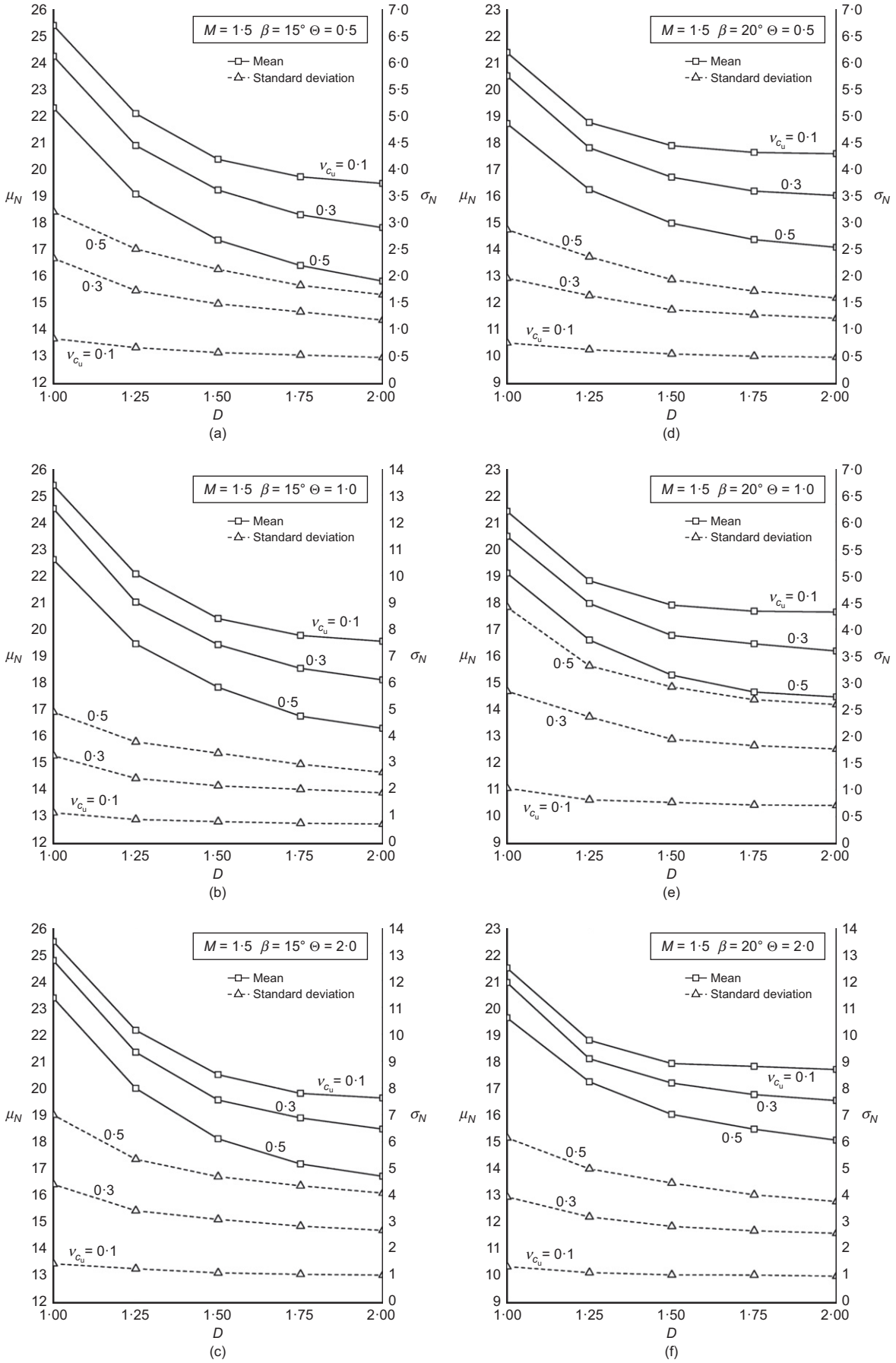

Fig. 5. Mean and standard deviation of stability number (μ_N and σ_N) against depth ratio (D) for M = 1·5: (a) β = 15° and Θ = 0·5; (b) β = 15° and Θ = 1·0; (c) β = 15° and Θ = 2·0; (d) β = 20° and Θ = 0·5; (e) β = 20° and Θ = 1·0; (f) β = 20° and Θ = 2·0; (g) β = 30° and Θ = 0·5; (h) β = 30° and Θ = 1·0; (i) β = 30° and Θ = 2·0; (j) β = 40° and Θ = 0·5; (k) β = 40° and Θ = 1·0; (l) β = 40° and Θ = 2·0 (continued on next page)

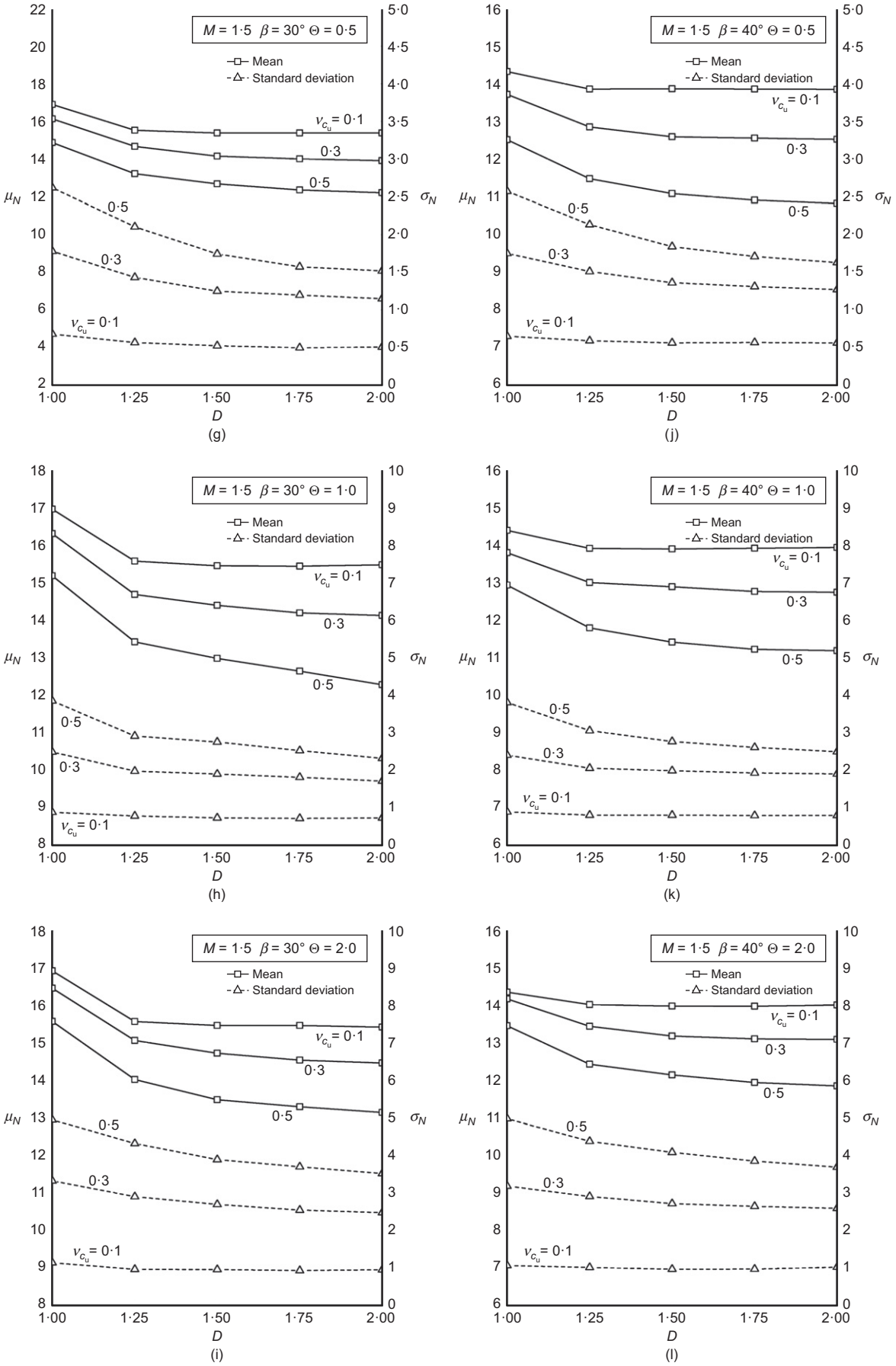

Fig. 5. Continued

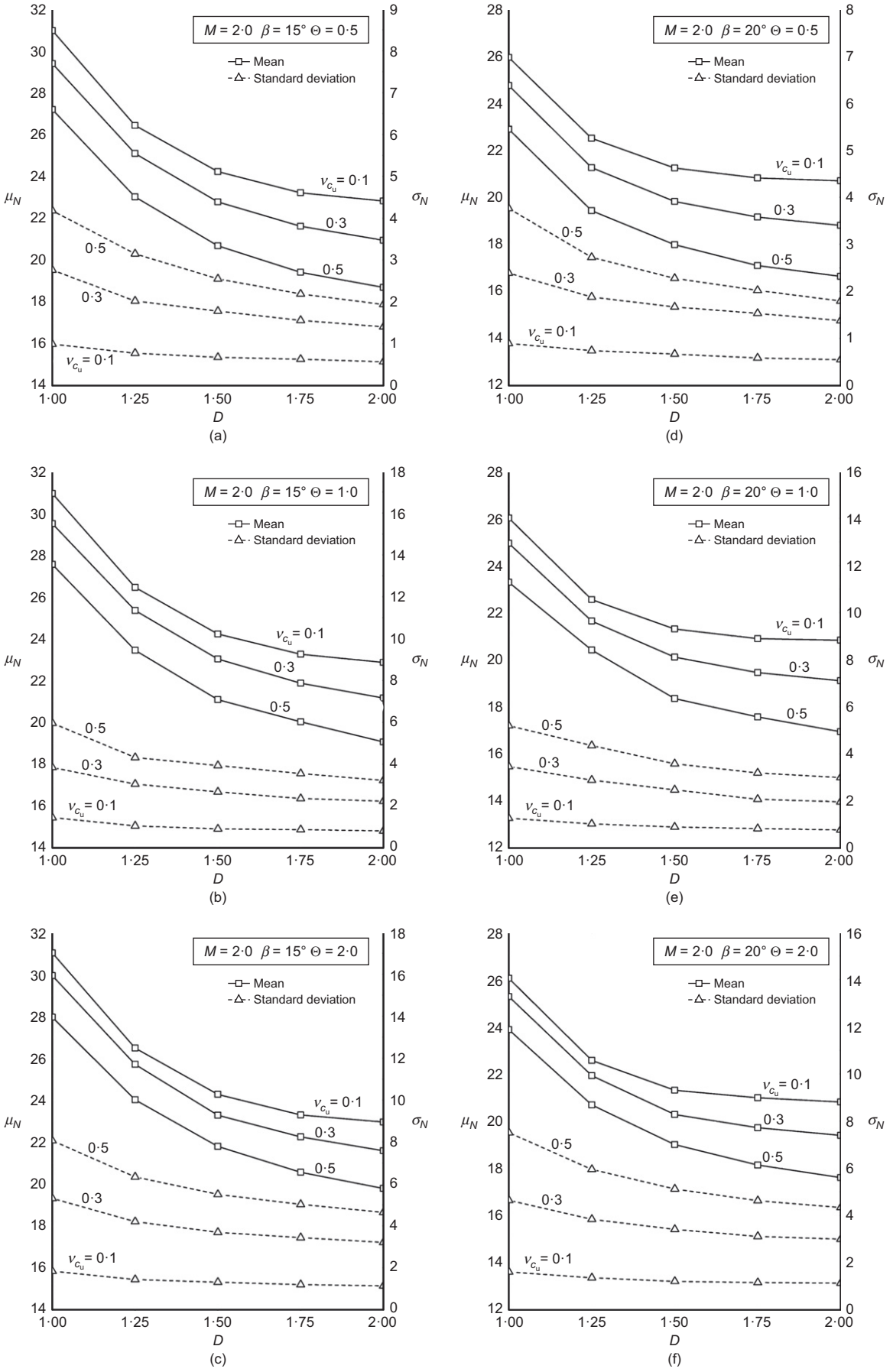

Fig. 6. Mean and standard deviation of stability number (μ_N and σ_N) against depth ratio (D) for $M = 2{\cdot}0$: (a) $\beta = 15°$ and $\Theta = 0{\cdot}5$; (b) $\beta = 15°$ and $\Theta = 1{\cdot}0$; (c) $\beta = 15°$ and $\Theta = 2{\cdot}0$; (d) $\beta = 20°$ and $\Theta = 0{\cdot}5$; (e) $\beta = 20°$ and $\Theta = 1{\cdot}0$; (f) $\beta = 20°$ and $\Theta = 2{\cdot}0$; (g) $\beta = 30°$ and $\Theta = 0{\cdot}5$; (h) $\beta = 30°$ and $\Theta = 1{\cdot}0$; (i) $\beta = 30°$ and $\Theta = 2{\cdot}0$; (j) $\beta = 40°$ and $\Theta = 0{\cdot}5$; (k) $\beta = 40°$ and $\Theta = 1{\cdot}0$; (l) $\beta = 40°$ and $\Theta = 2{\cdot}0$ (continued on next page)

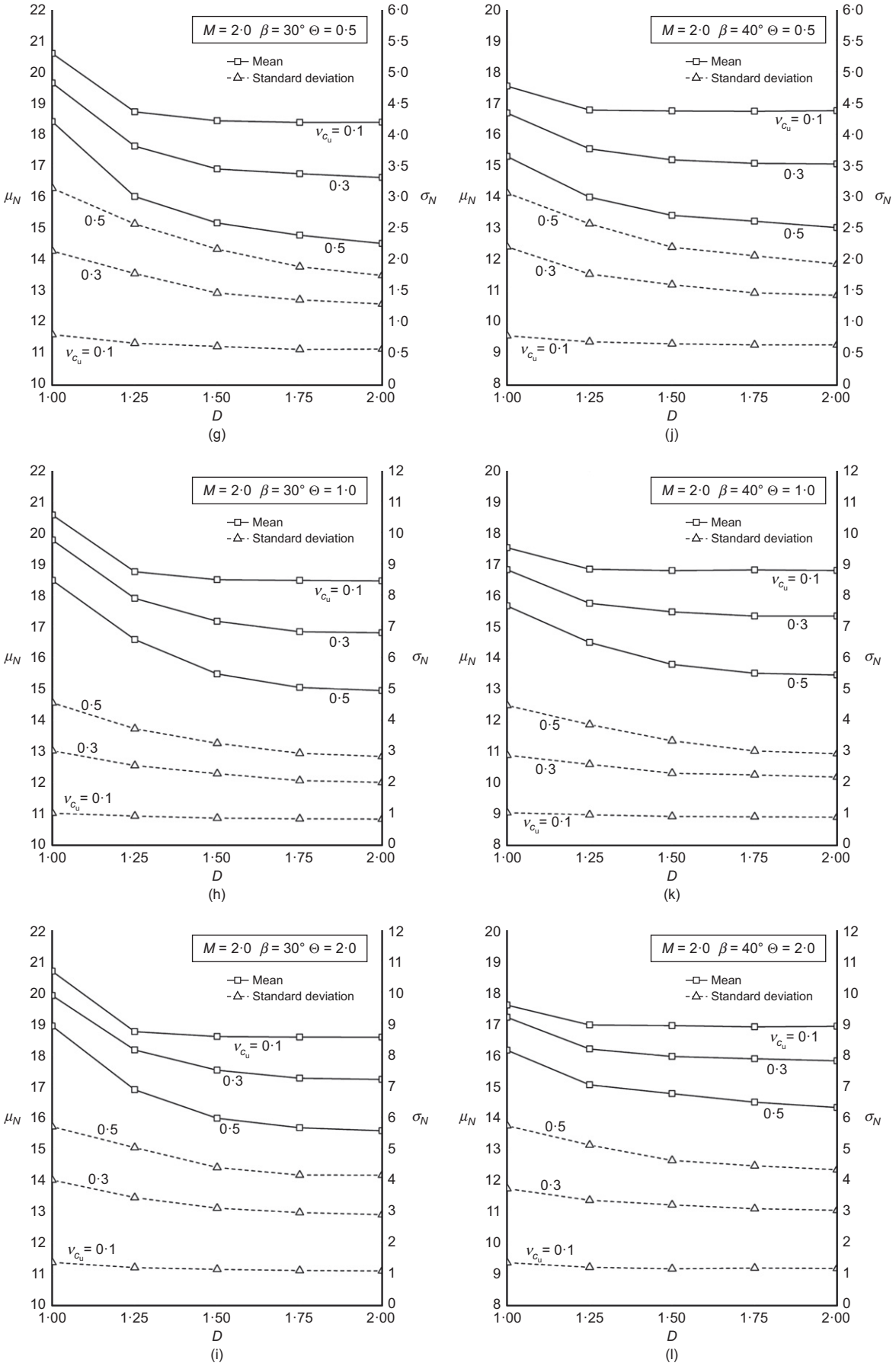

Fig. 6. Continued

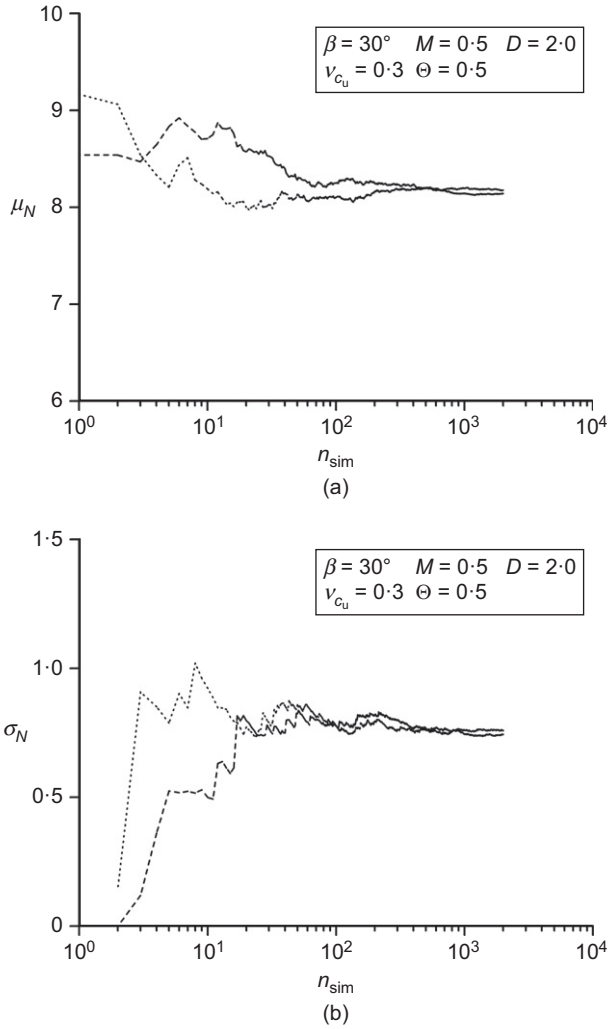

Fig. 7. Check on the number of Monte-Carlo simulations needed for stable results: (a) variation of μ_N with n_{sim}; (b) variation of σ_N with n_{sim}

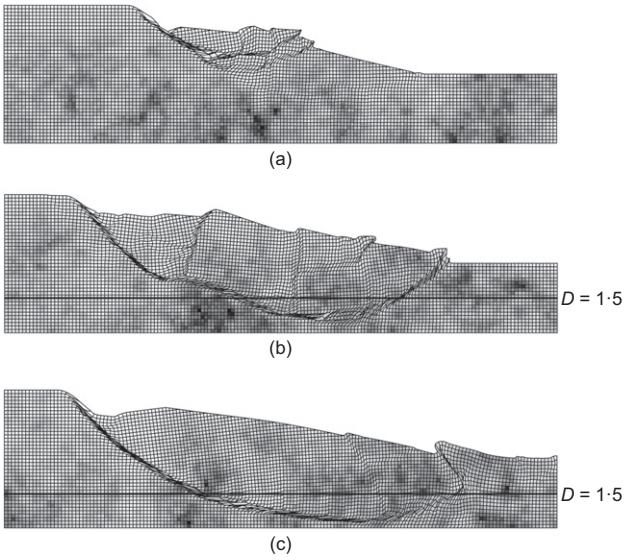

Fig. 9. Failure mechanisms for the case slope with $D = 2{\cdot}0$ and $v_{c_u} = 0{\cdot}5$: (a) shallow failure mechanism; (b) and (c) deep failure mechanism

deeper, as shown in Figs 9(b) and 9(c). This can happen probabilistically, however, because some random field simulations generate sufficiently low strengths in this deeper range to attract the critical mechanism. Recent studies by Ching *et al*. (2014, 2016) have also emphasised the importance of the 'seeking out' effect in RFEM.

As expected, Figs 3–6 also show the standard deviation of the stability number σ_N increasing as the input coefficient of variation is increased.

Example 1: Distribution of N *and* p_f *for a higher value of* v_{c_u}

As each non-stationary random field simulation computes a different stability number, N, the sample probability density function (pdf) of N values can be plotted for analysis. Fig. 10 shows a histogram of N values for an example slope problem with geometry and properties shown in Table 1, together with a lognormal fit. As shown in Fig. 10, the fitted curve agrees well with random field results. The histogram is obviously positive-skewed, and a goodness-of-fit test indicates that a p-value is about 0·45.

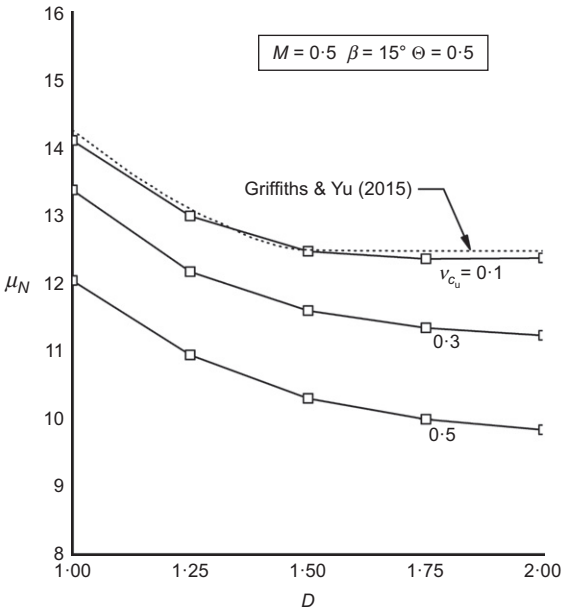

Fig. 8. Typical result for a slope with $M = 0{\cdot}5$, $\beta = 15°$ and $\Theta = 0{\cdot}5$

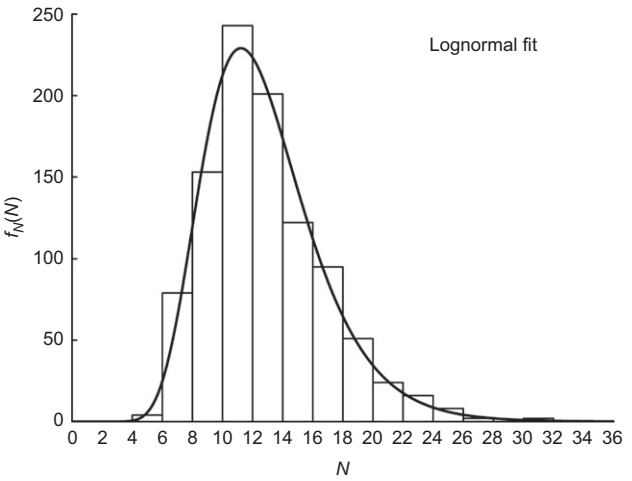

Fig. 10. Histogram and lognormal fit for example 1

Table 1. Geometry and properties for example 1

β: deg	H: m	D	$\mu_{c_{u0}}$: kPa	v_{c_u}	Θ	ρ: kN/m^3	γ: kN/m^3	M
15	10	1	15	0·5	2·0	3	20	0·5

Table 2. Geometry and properties for example 2

β: deg	H: m	D	$\mu_{c_{u0}}$: kPa	v_{c_u}	Θ	ρ: kN/m^3	γ: kN/m^3	M
15	10	1	20	0·3	2·0	1	20	2·0

Use of the charts is now demonstrated to estimate the probability of failure. Fig. 3(c) with $v_{c_u} = 0{\cdot}5$ (a suggested upper bound for the coefficient of variation of undrained strength; e.g. Lee *et al.* (1983); Phoon & Kulhawy (1999)) and $D = 1$, gives $\mu_N \approx 12{\cdot}81$ and $\sigma_N \approx 3{\cdot}91$. Assuming that N is lognormal, as suggested above, the standard deviation and mean of the underlying normal distribution of ln$N$ are given by

$$\sigma_{\ln N} = \sqrt{\ln\left(1 + v_N^2\right)} = \sqrt{\ln\left(1 + 0{\cdot}31^2\right)} = 0{\cdot}303 \tag{7}$$

$$\mu_{\ln N} = \ln \mu_N - \frac{1}{2}\sigma_{\ln N}^2 = \ln(12{\cdot}81) - \frac{1}{2}0{\cdot}303^2 = 2{\cdot}504 \tag{8}$$

Finally the probability of failure (p_f) is given by

$$\begin{aligned} p_f &= p[\mathrm{FS} < 1] = p\left[N\frac{\rho}{\gamma} < 1\right] = p\left[N\frac{3}{20} < 1\right] \\ &= p[N < 6{\cdot}67] = \Phi\left(\frac{\ln 6{\cdot}67 - \mu_{\ln N}}{\sigma_{\ln N}}\right) \\ &= \Phi\left(\frac{\ln 6{\cdot}67 - 2{\cdot}504}{0{\cdot}303}\right) = \Phi(-2{\cdot}00) \\ &= 1 - \Phi(2{\cdot}00) = 0{\cdot}023 \end{aligned} \tag{9}$$

where $\Phi(.)$ is the standard normal cumulative distribution function.

Example 2: Distribution of N *and* p_f *for an intermediate value of* v_{c_u}

In this example, an intermediate value of the coefficient of variation of undrained strength is adopted, with input parameters as shown in Table 2.

As shown in Fig. 11, a lognormal fit to the stability number N once more gives a good fit and the p-value for goodness of fit test is about 0·18. As might be expected, owing to the lower value of the coefficient of variation of v_{c_u} in this example, the degree of skewness of the histogram is less pronounced than that in Fig. 10.

The use of the charts is now illustrated for example 2.

Figure 6(c) with $v_{c_u} = 0{\cdot}3$ and $D = 1$ gives $\mu_N \approx 29{\cdot}93$ and $\sigma_N \approx 5{\cdot}31$. Parameters of the underlying normal distribution of ln$N$ are given from standard transformations as

$$\sigma_{\ln N} = \sqrt{\ln\left(1 + 0{\cdot}18^2\right)} = 0{\cdot}179 \tag{10}$$

$$\mu_{\ln N} = \ln(29{\cdot}93) - \frac{1}{2}0{\cdot}179^2 = 3{\cdot}383 \tag{11}$$

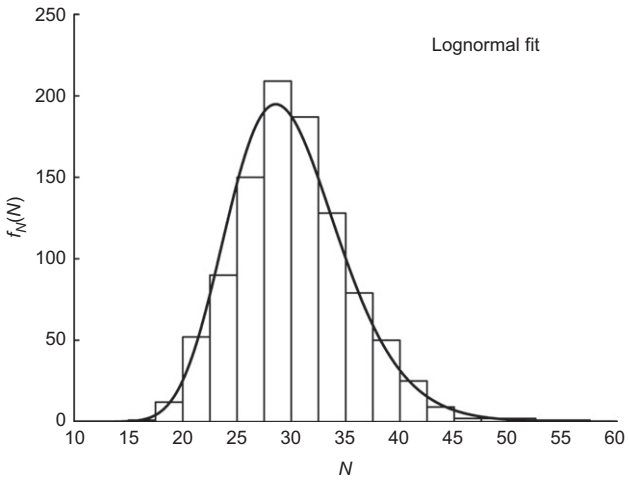

Fig. 11. Histogram and lognormal fit for example 2

The probability of failure is therefore given by

$$\begin{aligned} p_f &= p\left[N\frac{1}{20} < 1\right] = p[N < 20] = \Phi\left(\frac{\ln 20 - 3{\cdot}383}{0{\cdot}179}\right) \\ &= 1 - \Phi(2{\cdot}16) = 0{\cdot}015 \end{aligned} \tag{12}$$

CONCLUDING REMARKS

The note has described RFEM analyses of undrained slopes with non-zero mean strength at the ground surface and linearly increasing mean strength with depth. A constant coefficient of variation was assumed in the current work. An algorithm to generate the non-stationary random field for this normally consolidated clay slopes was proposed. Results have been presented for the mean stability number μ_N and standard deviation of stability number σ_N as a function of slope angle, β, depth ratio, D, coefficient of variation, v_{c_u}, dimensionless spatial correlation length, Θ, and strength gradient parameter, M. Although the values of μ_N for slopes with low values of the coefficient of variation were in good agreement with the recently published deterministic results of Griffiths & Yu (2015), for higher values of the coefficient of variation, μ_N fell below the deterministic lower bound as the depth ratio D was increased. This can be attributed to the 'seeking out' ability of finite-element slope stability analysis, where deeper failure mechanisms can be attracted to low strengths at greater depths generated by the random fields. Finally, use of the charts to estimate the probability of slope failure was illustrated through two examples. Engineers can

use the charts for preliminary assessment of the reliability of normally consolidated clay slopes with linearly increasing mean strength with depth.

ACKNOWLEDGEMENT

The first author was a visiting PhD student at Colorado School of Mines for the period of this research. The support of China Scholarship Council is acknowledged.

APPENDIX

Given that for any random variable X with lognormal distribution

$$\sigma_{\ln X} = \sqrt{\ln\left(1 + v_X^2\right)} \tag{13}$$

$$\mu_{\ln X} = \ln \mu_X - \sigma_{\ln X}^2/2 \tag{14}$$

Since v_{c_u} is constant

$$\sigma_{\ln c_{zi}} = \sigma_{\ln c_{0i}} \tag{15}$$

The relationship between c_{zi} and c_{0i} is therefore

$$\begin{aligned} c_{zi} &= \exp\left(\frac{\ln c_{0i} - \mu_{\ln c_{0i}}}{\sigma_{\ln c_{0i}}} \times \sigma_{\ln c_{zi}} + \mu_{\ln c_{zi}}\right) \\ &= \exp\left(\frac{\ln c_{0i} - \mu_{\ln c_{0i}}}{\sigma_{\ln c_{0i}}} \times \sigma_{\ln c_{0i}} + \mu_{\ln c_{zi}}\right) \\ &= \exp\left(\ln c_{0i} - \mu_{\ln c_{0i}} + \mu_{\ln c_{zi}}\right) \\ &= \exp\left(\ln c_{0i} - \mu_{\ln c_{0i}} + \ln \mu_{c_{zi}} - \frac{1}{2}\sigma_{\ln c_{zi}}^2\right) \\ &= \exp\left(\ln c_{0i} - \mu_{\ln c_{0i}} + \ln \mu_{c_{zi}} - \frac{1}{2}\sigma_{\ln c_{0i}}^2\right) \\ &= \exp\left(\ln c_{0i} - \ln \mu_{c_{0i}} + \ln \mu_{c_{zi}}\right) \\ &= c_{0i}\frac{\mu_{c_{zi}}}{\mu_{c_{0i}}} \end{aligned} \tag{16}$$

According to equation (1), $\mu_{c_{uz}} = \mu_{c_{u0}} + \rho z$. As the mean of initial values c_{0i} is $\mu_{c_{u0}}$, $\mu_{c_{0i}} = \mu_{c_{u0}}$, thus

$$c_{zi} = c_{0i}\frac{\mu_{c_{u0}} + \rho z}{\mu_{c_{u0}}} \tag{17}$$

NOTATION

c_{0i}	initial strength values
c_{zi}	strength values after adjustment
D	depth ratio
FS	factor of safety
H	slope height
H_0	height above crest where $\mu_{c_{u0}} = 0$
i	simple counter
M	strength gradient parameter
N	stability number
n	number of elements
n_{sim}	number of simulations
p	smallest value of α at which hypothesis would be rejected
p_f	probability of failure
v_{c_u}	coefficient of variation of strength
v_N	coefficient of variation of stability number
v_X	coefficient of variation of X
X	generic random variable
z	depth below crest
α	significance level
β	slope angle
γ	unit weight
Θ	dimensionless spatial correlation length
θ	spatial correlation length
$\mu_{c_{u0}}$	mean strength at the crest level
$\mu_{c_{uz}}$	mean strength at depth z
$\mu_{\ln N}$	mean of $\ln N$
$\mu_{\ln X}$	mean of $\ln X$
μ_N	mean of stability number
μ_X	mean value of X
ρ	strength gradient
$\sigma_{c_{u0}}$	standard deviation of strength at the crest level
$\sigma_{\ln N}$	standard deviation of $\ln N$
$\sigma_{\ln X}$	standard deviation of $\ln X$
σ_N	standard deviation of stability number
σ_X	standard deviation of X
$\Phi(.)$	standard normal cumulative distribution function
ϕ_u	total stress friction angle (= 0)

REFERENCES

Alonso, E. E. (1976). Risk analysis of slopes and its application to slopes in Canadian sensitive clays. *Géotechnique* **26**, No. 3, 453–472, http://dx.doi.org/10.1680/geot.1976.26.3.453.

Ching, J., Phoon, K. K. & Kao, P. H. (2014). Mean and variance of mobilized shear strength for spatially variable soils under uniform stress states. *J. Engng Mech., ASCE* **140**, No. 3, 487–501.

Ching, J., Hu, Y. G. & Phoon, K. K. (2016). On characterizing spatially variable soil shear strength using spatial average. *Probabilistic Engng Mech.* **45**, 31–43.

Christian, J. T., Ladd, C. C. & Baecher, G. B. (1994). Reliability applied to slope stability analysis. *J. Geotech. Engng, ASCE* **120**, No. 12, 2180–2207.

Duncan, J. M. (2000). Factors of safety and reliability in geotechnical engineering. *J. Geotech. Geoenviron. Engng, ASCE* **126**, No. 4, 307–316.

Fenton, G. A. & Griffiths, D. V. (1993). Statistics of block conductivity through a simple bounded stochastic medium. *Water Resources Res.* **29**, No. 6, 1825–1830.

Fenton, G. A. & Vanmarcke, E. H. (1990). Simulation of random fields via local average subdivision. *J. Engng Mech., ASCE* **116**, No. 8, 1733–1749.

Gibson, R. E. & Morgenstern, N. (1962). A note on the stability of cuttings in normally consolidated clay. *Géotechnique* **12**, No. 3, 212–216, http://dx.doi.org/10.1680/geot.1962.12.3.212.

Griffiths, D. V. & Fenton, G. A. (1993). Seepage beneath water retaining structures founded on spatially random soil. *Géotechnique* **43**, No. 4, 577–587, http://dx.doi.org/10.1680/geot.1993.43.4.577.

Griffiths, D. V. & Fenton, G. A. (2000). Influence of soil strength spatial variability on the stability of an undrained clay slope by finite elements. In *Slope stability 2000* (eds D. V. Griffiths, G. A. Fenton and T. R. Martin), GSP No. 101, pp. 184–193. Reston, VA, USA: American Society of Civil Engineers (ASCE).

Griffiths, D. V. & Fenton, G. A. (2004). Probabilistic slope stability analysis by finite elements. *J. Geotech. Geoenviron. Engng, ASCE* **130**, No. 5, 507–518.

Griffiths, D. V. & Yu, X. (2015). Another look at the stability of slopes with linearly increasing undrained strength. *Géotechnique* **65**, No. 10, 824–830, http://dx.doi.org/10.1680/jgeot.14.T.030.

Griffiths, D. V., Huang, J. & Fenton, G. A. (2009). Influence of spatial variability on slope reliability using 2-D random fields. *J. Geotech. Geoenviron. Engng, ASCE* **135**, No. 10, 1367–1398.

Griffiths, D. V., Huang, J. & Fenton, G. A. (2015). Probabilistic slope stability analysis using RFEM with non-stationary random fields. In *Geotechnical safety and risk V* (eds T. Schweckendiek, F. van Tol, D. Pereboom, M. van Staveren and P. Cools), pp. 704–709. Amsterdam, the Netherlands: IOS Press.

Hassan, A. M. & Wolff, T. F. (1999). Search algorithm for minimum reliability index of earth slopes. *J. Geotech. Geoenviron. Engng, ASCE* **125**, No. 4, 301–308.

Hicks, M. A. & Samy, K. (2002). Influence of heterogeneity on undrained clay slope stability. *Q. J. Engng Hydrogeol.* **35**, No. 1, 41–49.

Hunter, J. H. & Schuster, R. L. (1968). Stability of simple cuttings in normally consolidated clay. *Géotechnique* **18**, No. 3, 372–378, http://dx.doi.org/10.1680/geot.1968.18.3.372.

Koppula, S. D. (1984). On stability of slopes in clay with linearly increasing strength. *Can. Geotech. J.* **21**, No. 3, 577–581.

Lacasse, S. (1994). Reliability and probabilistic methods. *Proceedings of the 13th international conference on soil mechanics and foundation engineering*, New Delhi, India, pp. 225–227.

Lee, I. K., White, W. & Ingles, O. G. (1983). *Geotechnical engineering*. London, UK: Pitman.

Li, D., Qi, X., Phoon, K. K., Zhang, L. M. & Zhou, C. (2014). Effect of spatially variable shear strength parameters with linearly increasing mean trend on reliability of infinite slopes. *Struct. Saf.* **49**, 45–55.

Li, D., Qi, X., Cao, Z., Tang, X., Zhou, W., Phoon, K. K. & Zhou, C. (2015). Reliability analysis of strip footing considering spatially variable undrained shear strength that linearly increases with depth. *Soils Found.* **55**, No. 4, 866–880.

Lumb, P. (1966). The variability of natural soils. *Can. Geotech. J.* **3**, No. 2, 74–97.

Matsuo, M. & Kuroda, K. (1974). Probabilistic approach to the design of embankments. *Soils Found.* **14**, No. 1, 1–17.

Müller, R., Larsson, S. & Spross, J. (2016). Multivariate stability assessment during staged construction. *Can. Geotech. J.* **53**, No. 4, 608–618.

Phoon, K. K. & Kulhawy, F. H. (1999). Characterization of geotechnical variability. *Can. Geotech. J.* **36**, No. 4, 612–624.

Tang, W. H., Yucemen, M. S. & Ang, A. H. S. (1976). Probability-based short term design of slopes. *Can. Geotech. J.* **13**, No. 3, 201–215.

Terzaghi, K. (1948). Foreword to the inaugural volume of *Géotechnique*. *Géotechnique* **1**, No. 1, 3–5.

USACE (U.S. Army Corps of Engineers) (2003). *Engineering and design-slope stability, engineering manual EM 1110-2-1902*. Washington, DC, USA: Department of the Army, Corps of Engineers, Office of the Chief of Engineers.

Vanmarcke, E. H. (1977). Reliability of earth slopes. *J. Geotech. Engng Div.* **103**, No. 11, 1247–1265.

Whitman, R. V. (1984). Evaluating calculated risk in geotechnical engineering. *J. Geotech. Engng, ASCE* **110**, No. 2, 143–188.

Wolff, T. F. (1996). Probabilistic slope stability in theory and practice. In *Uncertainty in the geologic environment: from theory to practice* (eds C. D. Shackelford, P. P. Nelson and M. J. S. Roth), GSP No. 58, pp. 419–433. Reston, VA, USA: American Society of Civil Engineers (ASCE).

Yu, H. S., Salgado, R., Sloan, S. W. & Kim, J. M. (1998). Limit analysis versus limit equilibrium for slope stability. *J. Geotech. Geoenviron. Engng, ASCE* **124**, No. 1, 1–11.